Materials Science & Engineering A 727 (2018) 177–183

Contents lists available at ScienceDirect

Materials Science & Engineering A

journal homepage: www.elsevier.com/locate/msea

# Low-temperature superplasticity of nugget zone of friction stir welded Al-Mg alloy joint

T. Luo[a], D.R. Ni[a,*], P. Xue[a], Y.Z. Li[a], B.L. Xiao[a], Z.Y. Ma[a], M.J. Fu[b], X.H. Li[b], Y.S. Zeng[b,*]

[a] Shenyang National Laboratory for Materials Science, Institute of Metal Research, Chinese Academy of Sciences, 72 Wenhua Road, Shenyang 110016, China
[b] Metal Forming Technology Department, Beijing Aeronautical Manufacturing Technology Research Institute, Beijing 100024, China

ARTICLE INFO

*Keywords:*
Low-temperature superplasticity
Friction stir welding
Aluminum alloys
Grain boundary sliding

ABSTRACT

Commercial 5083Al rolled plates, 2.8 mm thick, were subjected to friction stir welding (FSW) with the aim of achieving low-temperature superplasticity (LTSP) in the nugget zone (NZ). Fine-grained microstructure with average grain sizes of 1.6 and 1.8 μm was obtained in the upper and lower parts of the NZ, respectively. The NZ was subjected to superplastic investigation at 250 and 300 °C. It was indicated that the upper and lower parts of the NZ exhibited similar LTSP values of 550–570% at 300 °C, much higher than those reported previously (< 300%) in friction stir processed 5083Al. This excellent LTSP was attributed to the extremely fine-grained microstructure and predominant high angle grain boundaries (> 84%). Grain boundary sliding was determined to be the dominant deformation mechanism, with grain boundary diffusion as the rate-controlling step.

## 1. Introduction

Due to its good corrosion resistance, good weldability, lower density, and moderately high strength, 5083Al is one of the most widely used aluminum alloys in the aerospace and automobile industries [1]. The pursuit of higher formability has led to a large number of investigations of the superplasticity of solution-strengthened Al-Mg alloys [2–6].

However, the widespread use of superplastic forming is hampered by the high deformation temperature, which demands a higher level of mold design and may lead to the loss of solutes from the surface layer and severe grain growth. Therefore, low-temperature superplasticity (LTSP) is becoming an effective solution, especially for components of high surface quality [7]. It has been proven that grain refinement in materials results in a decrease of the superplasticity temperature and better superplastic properties [8–11].

With the development of the aerospace and automobile industries, superplasticity of a single piece of metal plate cannot satisfy the demand of industrial applications. Much more attention is paid to the production of large-scaled complex parts by the integral forming method. A process combining superplastic forming and diffusion bonding (SPF/DB) has been used to produce unitized components with greater design flexibility as well as considerable weight reduction [12]. The SPF/DB process is mainly applied to titanium alloys [13,14], but is not suitable for Al alloys due to the hindrance to the DB of dense oxide films on the contact surfaces.

The most feasible route for overcoming this issue is to find a proper welding technique in place of DB for achieving integral forming of aluminum components by SPF. In this case, the key point is how to obtain superplasticity in the nugget zone (NZ) of the welded joints. Conventional fusion welding techniques usually result in coarse solidification microstructure and porosity in the NZs. Therefore, it is hard to achieve superplasticity in the NZs of fusion welded joints.

Friction stir welding (FSW), a solid-state welding technique, is quite useful for welding aluminum alloys with fine and equiaxed grains in the NZs, which are essential for achieving superplasticity of the joint. However, the study of LTSP in the NZs is quite limited. Friction stir processing (FSP), a development based on the basic principles of FSW, has been used to produce fine-grained microstructure with predominant high angle grain boundaries (HAGBs, misorientation ≥ 15°) [1–3,15]. Therefore, FSP is considered as an effective and economical technique for achieving LTSP [8,16].

Nonetheless, it is necessary to be aware of two points. Firstly, little attention has been paid to the superplasticity of FSP 5083Al [17,18], especially LTSP. To the best of our knowledge, the optimal LTSP of only 280% was achieved in FSP 5083Al at 250 °C and a strain rate of $1 \times 10^{-4}\ s^{-1}$ [2]. Secondly, even if LTSP of 5083Al can be achieved by FSP, this is not sufficient to guarantee that a similar superplasticity can also be obtained in the NZ of the FSW 5083Al joint because of the difference in microstructure between them. For instance, the abutting surfaces of the two metal plates to be joined by FSW would influence the material's plastic deformation and form some unique

* Corresponding authors.
*E-mail addresses:* drni@imr.ac.cn (D.R. Ni), yszeng@hotmail.com (Y.S. Zeng).

https://doi.org/10.1016/j.msea.2018.05.003
Received 2 March 2018; Received in revised form 30 April 2018; Accepted 2 May 2018
Available online 03 May 2018
0921-5093/ 

microstructures in the NZ, such as the "S" line and kissing bond [19]. Therefore, LTSP in the NZs of FSW aluminum joints cannot be simply represented by FSP.

LTSP in the NZ is very important for producing large-scale complex parts by SPF. At the same time, FSW is a useful technique for welding aluminum alloys with fine, equiaxed grains in the NZs, which are essential for achieving superplasticity of the joint. Based on the necessity and feasibility of achieving LTSP in the NZs via FSW, the objective of this study is (i) to achieve excellent LTSP in the NZ of FSW 5083Al joints and (ii) to elucidate the main superplastic deformation mechanism of FSW 5083Al.

## 2. Experimental

In this study, 2.8-mm-thick commercial 5083Al-O rolled plates with a nominal composition of Al-4.59Mg-0.74Mn-0.21Fe-0.07Cr-0.03Si (wt %) were used. As-received plates were friction stir welded along the rolling direction at a tool rotation rate of 400 rpm and a traverse speed of 50 mm $min^{-1}$. A steel tool with a concave shoulder 10 mm in diameter, a threaded conical pin 4 mm in root diameter, and 2.65 mm in length was used. The pin tool was tilted towards the trailing direction during FSW and the tilt angle is 2.5° with respect to the plate surface.

The specimens for microstructural examinations were cross-sectioned perpendicular to the welding direction. Microstructure characterization was performed by optical microscopy (OM), scanning electron microscopy (SEM), electron backscatter diffraction (EBSD) and transmission electron microscopy (TEM). The OM samples were mechanically ground, polished with 1.5 µm polishing paste, and then etched in 10 vol% phosphoric acid at 50 °C. EBSD analysis was carried out on a ZEISS SUPRA 55 scanning electric microscope (SEM) with an HKL Channel EBSD system at a step size of 0.1 µm. The fine microstructures of the welds were also examined by TEM (Tecnai 20). Specimens for EBSED and TEM were prepared by twin-jet polishing using a solution of 30% methanol and 70% nitric acid at −30 °C and 13 V.

It is well known that the NZ of the FSW joint can be divided into upper and lower regions due to the effect of the shoulder and pin, respectively, which might exhibit different microstructures [20]. Therefore, to evaluate the superplasticity accurately in the present study, the NZ was also divided into upper and lower regions, hereinafter referred to as NZ1 and NZ2, along the middle line of the plate thickness (Fig. 1). Two hardness profile lines corresponding to NZ1 and NZ2, respectively, with a distance of 0.7 mm from the upper and lower surfaces, were measured along the transverse cross-section of the welds at an interval of 1 mm. The hardness measurement was conducted on an automatic testing machine (Leco, LM-247AT) under a load of 500 g for 15 s.

Dog-bone shaped tensile specimens (2.5 mm gage length, 1.4 mm gage width, 1 mm thickness) were electro-discharge machined from NZ1 and NZ2, respectively, along the welding direction. Constant crosshead speed tensile tests were conducted at 300 °C and 250 °C, respectively, with four different initial strain rates ranging from $1 \times 10^{-4}$ $s^{-1}$ to $3 \times 10^{-3}$ $s^{-1}$, using an Instron 5848 microtester. It took 15 min for heating and stabilization of the temperature before starting the tensile test. The failed specimens were subjected to SEM examinations.

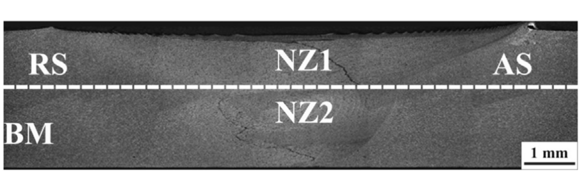


**Fig. 1.** Optical cross-sectional macrograph of FSW 5083Al joint.

## 3. Results and discussion

### 3.1. Microstructure evolution

Fig. 1 shows a cross-sectional OM macrograph of the FSW 5083Al joint. The entire NZ exhibits a basin shape with the typical characteristic "S" line. The widened upper region (NZ1) was formed by the extreme deformation due to the contact with the concave shoulder [21], while the lower region (NZ2) exhibiting the onion rings revealed the circular movement of the material and the extrusion effect induced by the pin.

Fig. 2 shows the OM, TEM, and SEM microstructures of the 5083Al base material (BM). It can be seen that along the rolling direction the microstructure was characterized by large elongated grains ~80 µm in length and ~18 µm in width (Fig. 2a). Rod-like phases dispersed in the grains were observed (Fig. 2b), and these phases should be $Al_6(MnFe)$, which was commonly reported in previous studies [22,23]. Meanwhile, a few coarse particles as large as 10 µm were found (Fig. 2c). EDS analysis showed that these phases were rich in Al, Mn, and Fe elements (Fig. 2d) and should be $Al_6(MnFe)$ particles which are the common impurity phases in 5083Al alloy.

TEM images showed that after FSW, the microstructure of the NZ was greatly refined, forming fine and equiaxed grains (Fig. 3). The grain sizes in both NZ1 and NZ2 were less than 2 µm. Fig. 4 shows the microstructure of NZ1 and NZ2 by EBSD mapping. The black and red lines represent the HAGBs and low angle grain boundaries (LAGBs, misorientation < 15°), respectively. Equiaxed recrystallized grains were observed in both regions; the average grain sizes were similar but a little larger in NZ1 (1.8 µm) than in NZ2 (1.6 µm).

As mentioned above, the thermal and mechanical processes were different in NZ1 and NZ2. For the thin sheet used in this study, the deformation in NZ1 was more severe, with a higher deformation rate, than that in NZ2, but the cooling rate in NZ2 was higher than that in NZ1. Therefore, a similar average grain size was obtained in NZ1 and NZ2 due to the combined thermal and deformation effect during FSW.

Fig. 5 shows the grain boundary misorientation angle distribution in NZ1 and NZ2. The statistics of the misorientation angles suggested that a high ratio of HAGBs was observed in both NZ1 (84%) and NZ2 (92%). Especially, the ratio of HAGBs in NZ2 is higher than that observed in FSP 5083Al by Charit and Mishra [1]. This typical microstructure with a high ratio of HAGBs was also found in other FSW/FSP aluminum alloys [3,8,9,21,24,25]. The fine-grained microstructure with a high ratio of HAGBs in the NZ was produced by the dynamic recrystallization due to the heat effect and plastic deformation during FSW [26–28].

### 3.2. Hardness distribution

Fig. 6 shows the microhardness profiles of both NZ1 and NZ2. It can be seen that the BM exhibited low hardness due to its annealed "O" condition, which was about 75–80 HV. After FSW, the hardness of the NZ was greatly increased, mainly owing to the effect of grain refinement, with peak values of about 95 HV in both NZ1 and NZ2. The width of the peak value zone on the line of NZ1 is about 10 mm and the zone on the line of NZ2 is a little narrower, corresponding to the different widths of the two regions.

### 3.3. Low-temperature superplasticity (LTSP)

#### 3.3.1. LTSP behavior of FSW 5083Al

Fig. 7a shows the variation of elongation with the initial strain rate and temperature for NZ1 and NZ2. It can be seen that both regions exhibited superplasticity at 250 and 300 °C. Corresponding to the similar microstructure features between NZ1 and NZ2, such as the HAGB ratio and grain size, there is no obvious difference in superplasticity between NZ1 and NZ2. Both regions exhibited a maximum elongation of around ~570% at the initial strain rate of $3 \times 10^{-4}$ $s^{-1}$ and 300 °C.

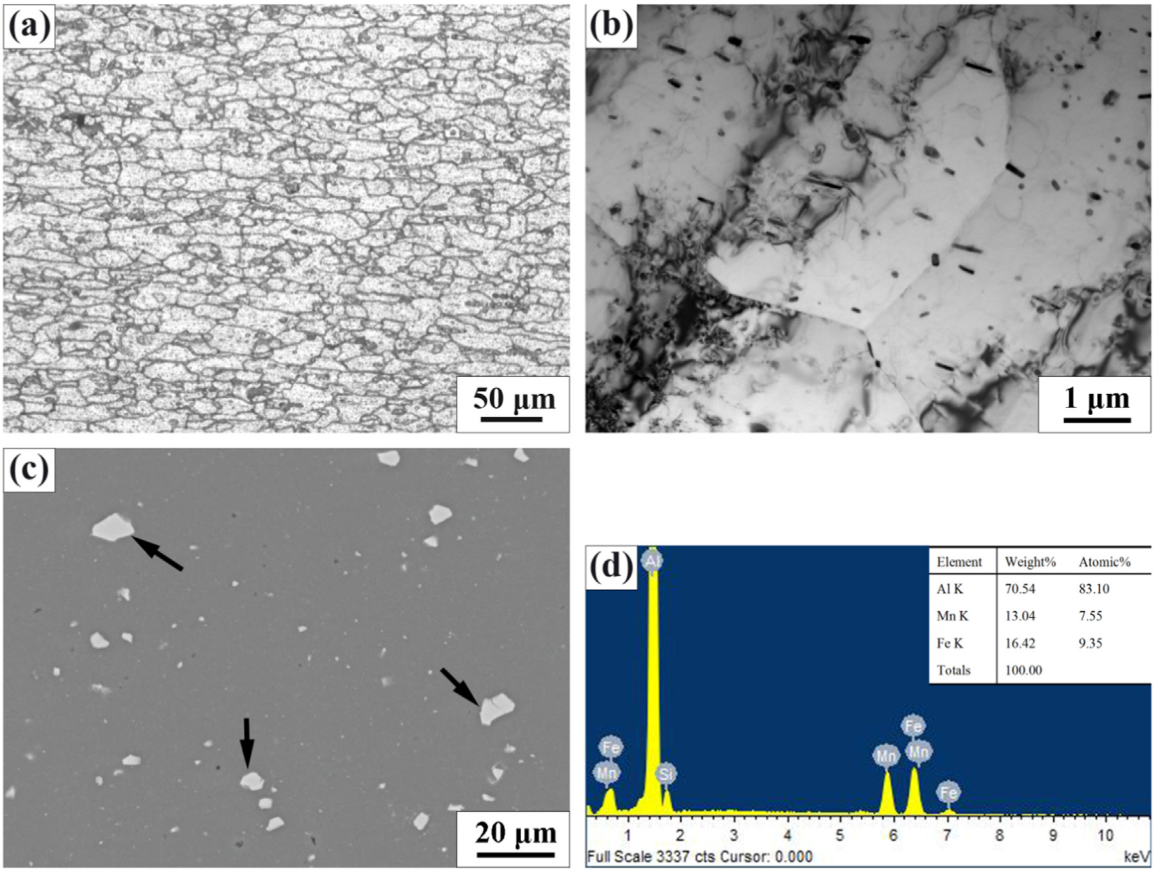


**Fig. 2.** Microstructures of 5083Al base material: (a) OM micrograph, (b) TEM bright field image, (c) SEM micrograph, and (d) EDS of $Al_6(MnFe)$ impurity.

Compared with the maximum ductility of 575% obtained at $3 \times 10^{-4}\ s^{-1}$ and 490 °C by Charit and Mishra [1] in FSP 5083Al, the temperature in this study decreased by 190 °C. This satisfying LTSP is very important for producing large-scaled components by the integral forming method. The elongation was reduced when the temperature decreased from 300° to 250 °C. At 250 °C, the largest elongation of 385% was obtained at the initial strain rate of $1 \times 10^{-4}\ s^{-1}$, which was much higher than that (285%) achieved in fine-grained (0.95 μm) FSP 5083Al with 72% HAGBs by El-Danaf et al. [2].

The flow stress (at true strain of 0.1) is plotted as a function of the initial strain rate on double logarithmic scales in Fig. 7b. The strain rate sensitivity ($m$) of FSW samples ranged from 0.34 to 0.49 at 300 °C and from 0.20 to 0.67 at 250 °C. At high temperatures, the grain-size independent, solute-drag-limited dislocation-glide mechanism with an $m$ value of ~0.33 is dominant in Al-Mg alloys while a typical $m$ value of ~0.5 usually indicates that the grain boundary sliding (GBS) is the

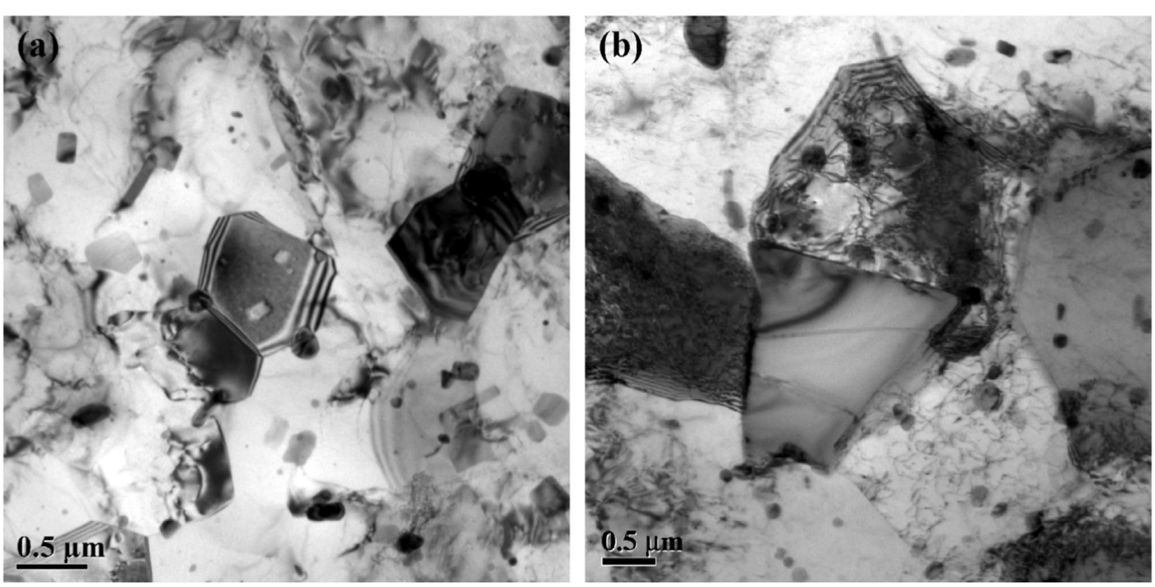


**Fig. 3.** TEM brightfield images of FSW 5083Al joint: (a) NZ1, (b) NZ2.

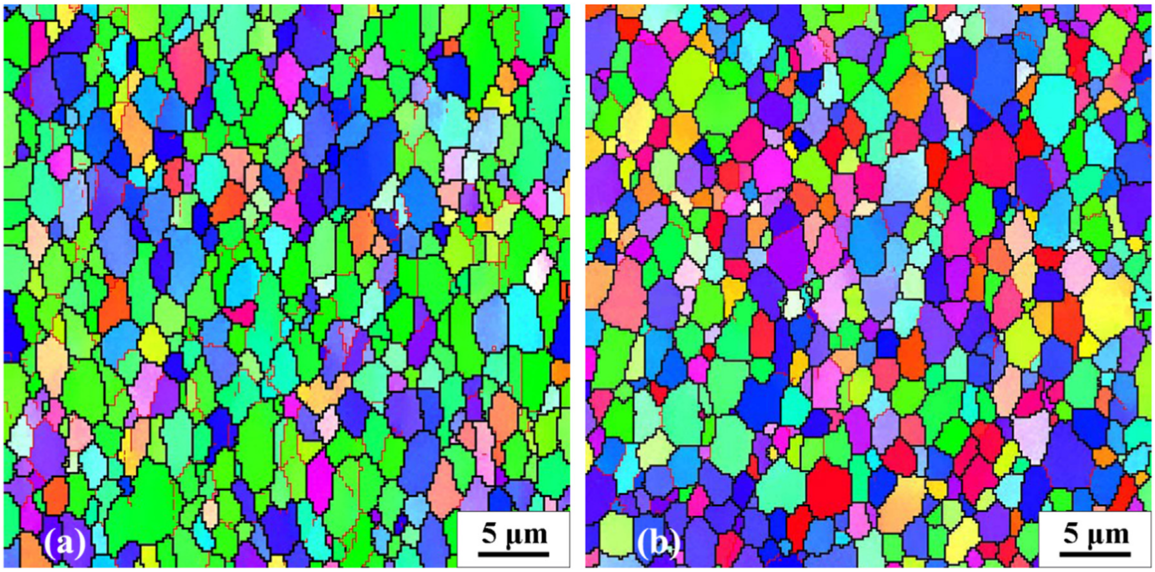


**Fig. 4.** EBSD images of FSW 5083Al joint: (a) NZ1, (b) NZ2.

dominant superplastic deformation mechanism in fine-grained materials. However, several previous studies [7,9,29] showed that GBS is an important deformation mechanism even though the measured *m* value is ~0.3, which is lower than the typical *m* value (~0.5) for GBS. Liu and Ma [9] suggested that GBS was the dominant mechanism while *m* values of 0.33–0.42 were observed for maximum superplasticity at low temperatures of 200–350 °C in FSP Al-Zn-Mg-Cu alloy.

Fig. 8 shows the failed tensile specimens which exhibited the maximum elongation at 300 and 250 °C, respectively. Uniform elongation was observed in all samples, which is the characteristic of superplastic flow [9].

### 3.3.2. LTSP mechanism of FSW 5083Al

The constitutive equation of the typical deformation behavior of polycrystalline material is given by [30,31]:

$$\dot{\varepsilon} = A\frac{D0Eb}{kT}\exp\left(-\frac{Q}{RT}\right)\left(\frac{b}{d}\right)^{p}\left(\frac{\sigma-\sigma_0}{E}\right)^{n} \tag{1}$$

where $\dot{\varepsilon}$ is the strain rate, $A$ is a constant, $D_O$ is the pre-exponential factor for diffusion, $E$ is the Young's modulus, $b$ is the Burger's vector, $k$ is the Boltzmann's constant, $T$ is the absolute temperature, $Q$ is the activation energy depending on the rate-controlling process, $R$ is the gas constant, $d$ is the grain size, $\sigma$ is the applied stress, $\sigma_O$ is the threshold stress, $p$ is the grain size exponent, and $n$ is the stress exponent. Three variables, $n$, $p$, and $Q$, are most important for determining the

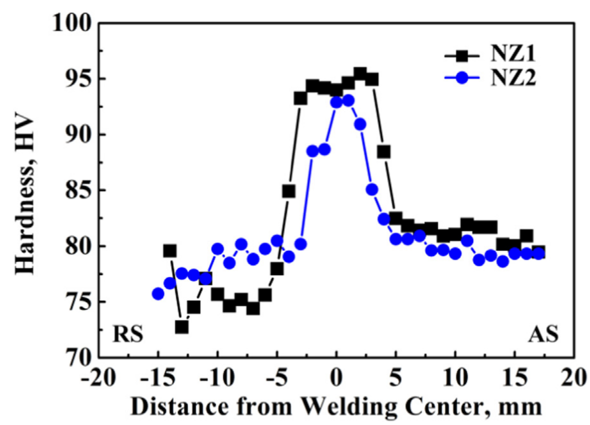


**Fig. 6.** Vickers hardness profiles of FSW 5083Al joint.

deformation mechanism.

In the present study of FSW 5083Al, the *m* value is smaller than the typical value of 0.5 for GBS and tends to increase with increases in the strain rate, which have also been observed in other studies [2,32]. This kind of *m* variation trend indicates either the operation of threshold stress or a change in the deformation mechanism during the superplastic deformation. The lower *m* values observed are more likely due to

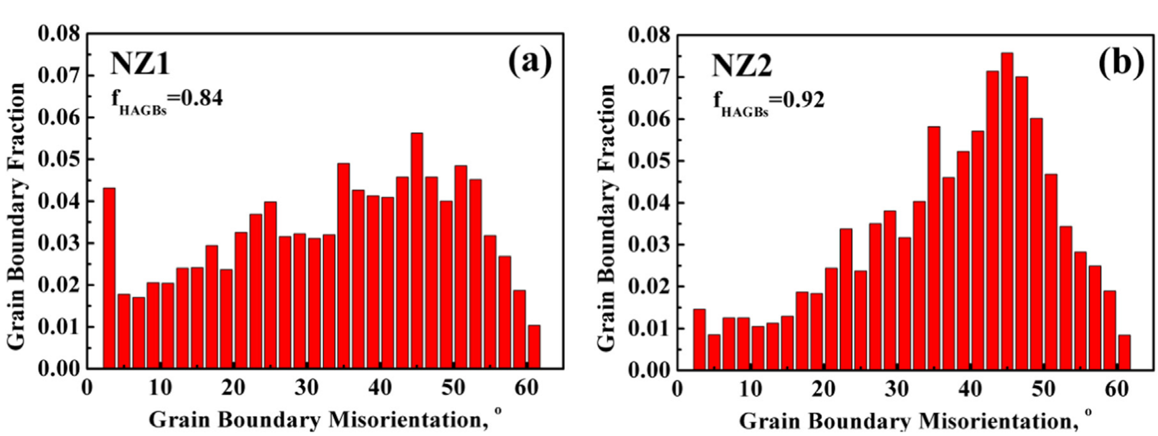


**Fig. 5.** Grain boundary misorientation angle distribution in FSW 5083Al joint: (a) NZ1, (b) NZ2.

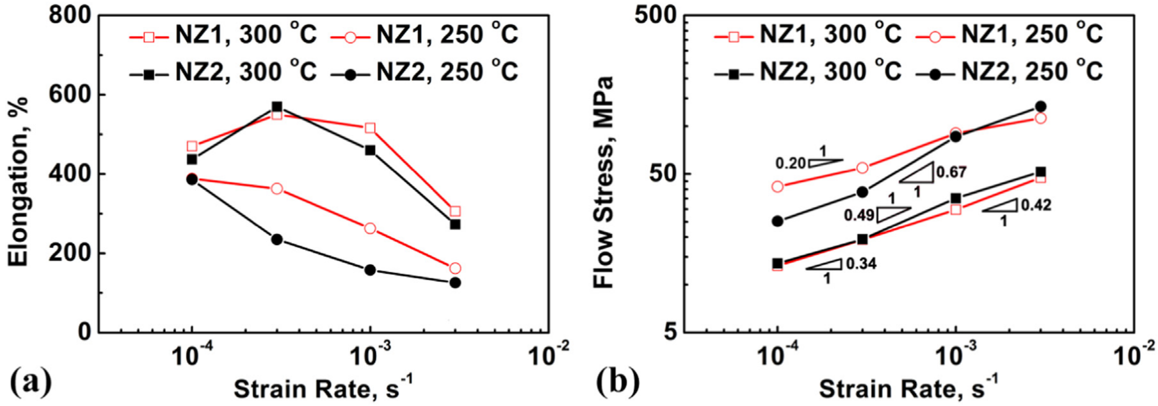


**Fig. 7.** Variation of (a) elongation and (b) flow stress with initial strain rate for FSW 5083Al joint.

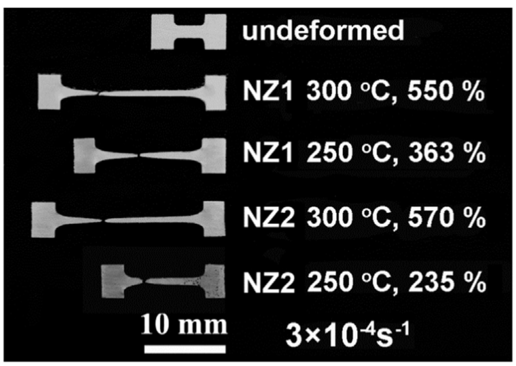


**Fig. 8.** Appearance of specimens before and after superplastic deformation at different temperatures of FSW 5083Al joint.

the existence of a threshold stress [32,33]. This existence of the threshold stresses was also reported based on the superplastic data analysis [34] and could be determined if the superplastic deformation mechanism could be deduced.

Fig. 9 shows the surface morphology of the tensile specimens deformed to failure for maximum superplasticity at 300 °C and 250 °C. Out-of-plane GBS and cavities could be observed on the surfaces of the tensile specimens. Between the sliding grains, some fibers (whiskers) or deformation-induced cavities were detected as indicated by the arrows in Fig. 9. Previously, the fibers were generally thought to develop due to the existence of liquid phases [35,36]. However, the fibers were detected in the present FSW 5083Al deformed at 300 and 250 °C. It is impossible to form the liquid phases. In other studies, the fibers were only formed with the existence of oxygen and composed of Mg-rich oxide [37–39]. Especially, Rust and Todd [37] believed that ligaments and whiskers in tension were developed from the striated region, which is part of the accommodation mechanism of the GBS. Therefore, in the present study, within the investigated temperature range, it was deduced from the surface morphology of tensile specimens, as shown in Fig. 9, that GBS was the primary superplastic deformation mechanism. Accordingly, the threshold stress could be determined because it was responsible for the change in the $m$ values [32].

In order to estimate the value of threshold stress and get an accurate modified value of $m$, a plot of σ against $(\dot{\varepsilon})^{1/n}$ ($n = 1, 2, 3, 5$; $n$ is the stress exponent and a reciprocal of $m$) on double-linear scales was adopted for this analysis. The results showed that $n = 2$ achieves the best fit for both NZ1 and NZ2 at 300 and 250 °C. So the modified value of $m$ is 0.5, which is the classical value representing the mechanism of GBS in superplastic deformation. The values of threshold stress were estimated by extrapolating the strain rate to zero as shown in Fig. 10a and b. The calculated values of threshold stress decrease with increasing temperature from 250° to 300 °C for both NZ1 and NZ2.

The activation energy ($Q$) indicating the rate-controlling process is another crucial factor in the determination of the deformation mechanism. It can be calculated by [40]:

$$Q = nR\frac{\partial \ln(\sigma - \sigma 0)}{\partial(1/T)}|\dot{\varepsilon} \tag{2}$$

The estimated values of $Q$ under a constant strain rate based on Eq. (2) were 88 and 85 kJ/mol for NZ1 and NZ2, respectively. These values are much lower than the activation energy for the lattice self-diffusion of pure Al (142 kJ/mol) but close to that for the grain boundary diffusion (84 kJ/mol). Therefore, on the basis of the estimated values of $Q$ and modified $m$, the dominant superplastic deformation mechanism is GBS with the grain boundary diffusion as the rate-controlling step.

As this study was conducted for one parameter, it is not possible to draw a plot of $\ln(\dot{\varepsilon})$ against $\ln(b/d)$ to estimate the value of the grain size exponent ($p$). However, the GBS models proposed by Arieli and Mukherjee [41] and the summarized experimental data by Langdon [42] suggested a stress exponent of 2, an activation energy close to that for grain boundary diffusion and a grain size dependence of 2. Thus $p$ is taken to be 2 here.

The contributions of the grain boundary diffusion and lattice diffusion depend on the microstructure and experimental conditions. In Harrison's classification [43], the diffusion regimes in a polycrystalline material are divided into three types: strong penetration in the whole grain volume (Type A), strong penetration in the grain boundary with a non-negligible lattice diffusion (Type B), and penetration only along the grain boundary (Type C). With the increase of the experimental time, the diffusion behavior may change from Type C to Type B and ultimately to Type A.

In this study, the value of $\sqrt{D_L t}$ ($D_L$ is the lattice diffusion coefficient; $t$ is the diffusion time) is just between the values of grain boundary width ($\delta$) and grain size ($d$), which indicates that the diffusion behavior belongs to type B. Unlike the diffusion driven by the gradient of chemical potential [43,44], the extra stress and the long experiment time of the superplastic deformation produced more vacancies and accelerated the lattice diffusion. Even though the grain boundary diffusion is still dominant, it is reasonable to consider the contribution of lattice diffusion. So we use an effective diffusion coefficient ($D_{eff}$), which was proposed by Sherby and Wadsworth [45] for the analysis of superplastic flow. It is expressed by a combination of the grain boundary diffusion coefficient ($D_{gb}$) and the lattice diffusion coefficient ($D_L$) as follows [46]:

$$D_{eff} = D_L + x\left(\frac{\pi}{d}\right)\delta D_{gb} \tag{3}$$

where $\delta$ is the grain boundary width with an approximate value of $2b$ and $x$ is an unknown constant. Here $D_{eff}$ is taken to be $[D_L + 1.72 \times 10^{-2}(\pi\delta/d)D_{gb}]$ [46].

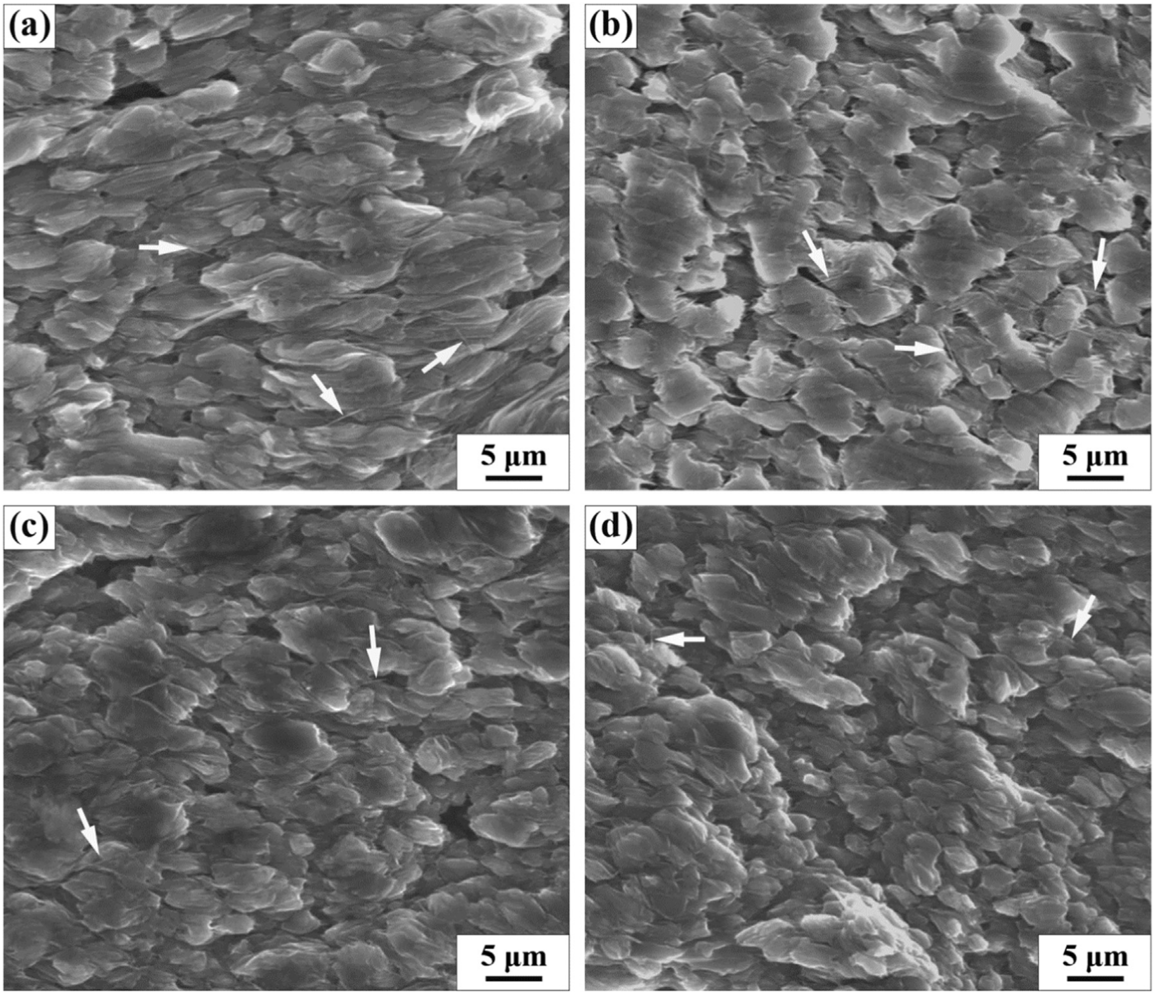


**Fig. 9.** Surface morphology of tensile specimens of FSW 5083Al joint near fracture tip after superplastic deformation to failure at (a) 300 °C, $3 \times 10^{-4}$ $s^{-1}$, NZ1; (b) 300 °C, $3 \times 10^{-4}$ $s^{-1}$, NZ2; (c) 250 °C, $1 \times 10^{-4}$ $s^{-1}$, NZ1; (d) 250 °C, $1 \times 10^{-4}$ $s^{-1}$, NZ2.

To further elucidate the superplastic deformation mechanism in FSW 5083Al, the variation of $(\dot{\varepsilon}kTd^2/D_{\mathrm{eff}}Eb^3)$ as a function of $(\sigma - \sigma_0)/E$ is shown in Fig. 11. It can be seen that all the data in this study can be represented by a straight line with a slope of 2. Thus, GBS is the main superplastic deformation mechanism for the present FSW 5083Al and the estimated $A$ value in the constitutive equation is equal to $3 \times 10^5$.

## 4. Conclusions

(1) Fine-grained microstructure with grain sizes of 1.6 and 1.8 µm in the upper nugget zone (NZ1) and lower nugget zone (NZ2), respectively, was obtained in the FSW 5083Al. High ratios of HAGBs were achieved in both two regions (84% for NZ1 and 92% for NZ2).
(2) The FSW 5083Al exhibited excellent low-temperature superplasticity at 300 and 250 °C, with NZ1 and NZ2 having similar superplastic elongations. Maximum superplasticity of > 550% was

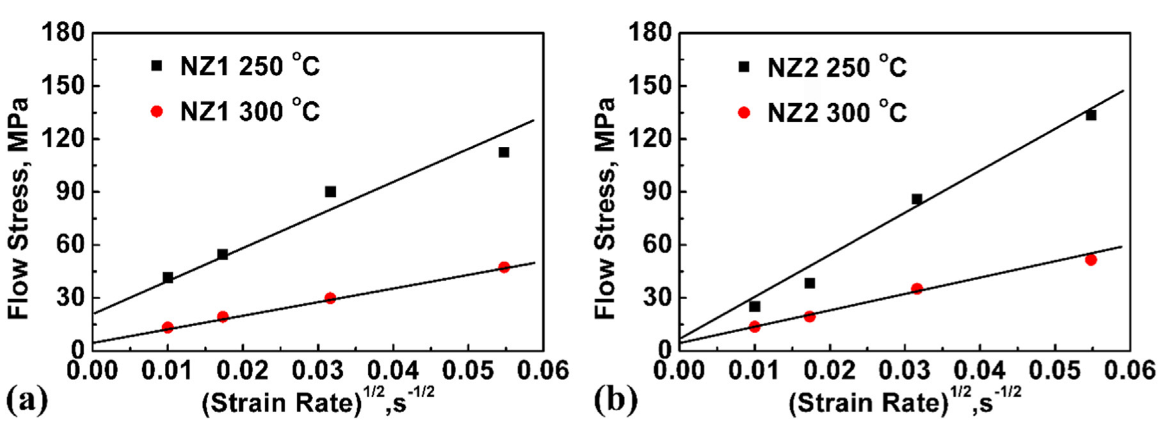


**Fig. 10.** Variation of flow stress as a function of $(\dot{\varepsilon})^{1/2}$ of (a) NZ1 and (b) NZ2 for FSW 5083Al joint.

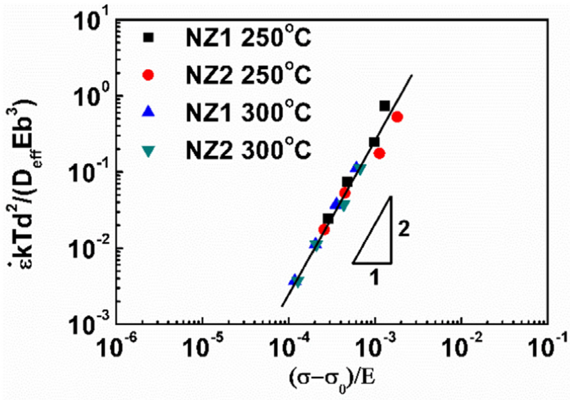


**Fig. 11.** Variation of ($\dot{\varepsilon}kTd^2/D_{\mathrm{eff}}Eb^3$) as a function of $(\sigma-\sigma_0)/E$ of NZ1 and NZ2 for FSW 5083Al joint.

observed in both NZ1 and NZ2 at $3 \times 10^{-4}$ $s^{-1}$ and 300 °C.

(3) The surface observations of deformed specimens provided evidence of grain boundary sliding. The analysis of the superplastic data indicates that grain boundary sliding is the dominant deformation mechanism with grain boundary diffusion as the rate-controlling step.

## Acknowledgments

This work was supported by the National Natural Science Foundation of China under Grant no. 51331008.

## References

[1] I. Charit, R.S. Mishra, J. Mater. Res. 19 (2004) 3329–3342.
[2] E.A. El-Danaf, M.M. El-Rayes, M.S. Soliman, Bull. Mater. Sci. 34 (2011) 1447–1453.
[3] M.A. García-Bernal, R.S. Mishra, R. Verma, D. Hernández-Silva, Mater. Sci. Eng. A 534 (2012) 186–192.
[4] R. Kaibyshev, F. Musin, D.R. Lesuer, T.G. Nieh, Mater. Sci. Eng., A 342 (2003) 169–177.
[5] S. Malopheyev, S. Mironov, I. Vysotskiy, R. Kaibyshev, Mater. Sci. Eng., A 649 (2016) 85–92.
[6] F.C. Liu, Z.Y. Ma, F.C. Zhang, J. Mater. Sci. Technol. 28 (2012) 1025–1030.
[7] I. Charit, R.S. Mishra, Acta Mater. 53 (2005) 4211–4223.
[8] F.C. Liu, Z.Y. Ma, L.Q. Chen, Scr. Mater. 60 (2009) 968–971.
[9] F.C. Liu, Z.Y. Ma, Scr. Mater. 58 (2008) 667–670.
[10] C. Yang, J.J. Wang, Z.Y. Ma, D.R. Ni, M.J. Fu, X.H. Li, Y.S. Zeng, Acta Metall. Sin. 51 (2015) 1449–1456.
[11] R. Verma, P.A. Friedman, A.K. Ghosh, S. Kim, C. Kim, Metall. Mater. Trans. A 27 (1996) 1889–1898.
[12] I. Charit, R.S. Mishra, M.W. Mahoney, Scr. Mater. 47 (2002) 631–636.
[13] D.G. Sanders, M. Ramulu, J. Mater. Eng. Perform. 13 (2004) 744–752.
[14] R.V. Safiullin, O. Rudenko, F.U. Enikeev, R.Y. Lutfullin, Mater. Sci. Forum, 1984 Trans Tech Publications, Aedermannsdorf, Switzerland, 1997, pp. 769–774.
[15] Z.A. Luo, G.M. Xie, Z.Y. Ma, G.L. Wang, G.D. Wang, J. Mater. Sci. Technol. 29 (2013) 1116–1122.
[16] Z.Y. Ma, R.S. Mishra, Scr. Mater. 53 (2005) 75–80.
[17] M.A. García-Bernal, R.S. Mishra, D. Hernández-Silva, V.M. Sauce-Rangel, J. Mater. Eng. Perform. 26 (2017) 460–464.
[18] L.B. Johannes, I. Charit, R.S. Mishra, R. Verma, Mater. Sci. Eng., A 464 (2007) 351–357.
[19] P.L. Threadgill, A.J. Leonard, H.R. Shercliff, P.J. Withers, Int. Mater. Rev. 54 (2009) 49–93.
[20] Y.Z. Li, Q.Z. Wang, B.L. Xiao, Z.Y. Ma, J. Mater. Process. Technol. 251 (2018) 305–316.
[21] Y.S. Sato, H. Kokawa, M. Enomoto, S. Jogan, Metall. Mater. Trans. A 30 (1999) 2429–2437.
[22] R. Goswami, R.L. Holtz, Metall. Mater. Trans. A 44 (2013) 1279–1289.
[23] J. Yan, A.M. Hodge, J. Alloy. Compd. 703 (2017) 242–250.
[24] D.P. Field, T.W. Nelson, Y. Hovanski, K.V. Jata, Metall. Mater. Trans. A 32 (2001) 2869–2877.
[25] P.B. Prangnell, C.P. Heason, Acta Mater. 53 (2005) 3179–3192.
[26] J.-Q. Su, T.W. Nelson, C.J. Sterling, Mater. Sci. Eng., A 405 (2005) 277–286.
[27] C.Y. Liu, B. Qu, P. Xue, Z.Y. Ma, K. Luo, M.Z. Ma, R.P. Liu, J. Mater. Sci. Technol. 34 (2018) 112–118.
[28] B.B. Wang, F.F. Chen, F. Liu, W.G. Wang, P. Xue, Z.Y. Ma, J. Mater. Sci. Technol. 33 (2017) 1009–1014.
[29] R.K. Islamgaliev, N.F. Yunusova, R.Z. Valiev, N.K. Tsenev, V.N. Perevezentsev, T.G. Langdon, Scr. Mater. 49 (2003) 467–472.
[30] R.S. Mishra, T.R. Bieler, A.K. Mukherjee, Acta Metall. Mater. 43 (1995) 877–891.
[31] R.S. Mishra, T.R. Bieler, A.K. Mukherjee, Acta Mater. 45 (1997) 561–568.
[32] Z.Y. Ma, F.C. Liu, R.S. Mishra, Acta Mater. 58 (2010) 4693–4704.
[33] P.K. Chaudhury, F.A. Mohamed, Acta Metall. 36 (1988) 1099–1110.
[34] Z.Y. Ma, R.S. Mishra, M.W. Mahoney, R. Grimes, Metall. Mater. Trans. A 36 (2005) 1447–1458.
[35] Y. Takayama, T. Tozawa, H. Kato, Acta Mater. 47 (1999) 1263–1270.
[36] C.L. Chen, M.J. Tan, Mater. Sci. Eng., A 298 (2001) 235–244.
[37] M.A. Rust, R.I. Todd, Acta Mater. 59 (2011) 5159–5170.
[38] R.B. Grishaber, R.S. Mishra, A.K. Mukherjee, Mater. Sci. Eng., A 220 (1996) 78–84.
[39] J.-K. Chang, E.M. Taleff, P.E. Krajewski, J.R. Ciulik, Scr. Mater. 60 (2009) 459–462.
[40] I.C. Hsiao, J.C. Huang, Metall. Mater. Trans. A 33 (2002) 1373–1384.
[41] A. Arieli, A.K. Mukherjee, Mater. Sci. Eng., A 45 (1980) 61–70.
[42] T.G. Langdon, Acta Metall. Mater. 42 (1994) 2437–2443.
[43] L.G. Harrison, Trans. Faraday Soc. 57 (1961) 1191–1199.
[44] R.A. De Souza, M. Martin, MRS Bull. 34 (2011) 907–914.
[45] O.D. Sherby, J. Wadsworth, G. Krauss (Ed.), Deformation, Processing and Structure, ASM, Metals Park, OH, 1984, pp. 355–388.
[46] H. Somekawa, T. Tanaka, H. Sasaki, K. Kita, A. Inoue, K. Higashi, Acta Mater. 52 (2004) 1051–1059.